

pubs.acs.org/JPCB Article

Post-translational Modifications of Cyclophilin D Fine-Tune Its Conformational Dynamics and Activity: Implications for Its Mitochondrial Function

Published as part of The Journal of Physical Chemistry virtual special issue "Jose Onuchic Festschrift". Jacques Kumutima, Xin-Qiu Yao, and Donald Hamelberg*



Cite This: J. Phys. Chem. B 2022, 126, 10844–10853



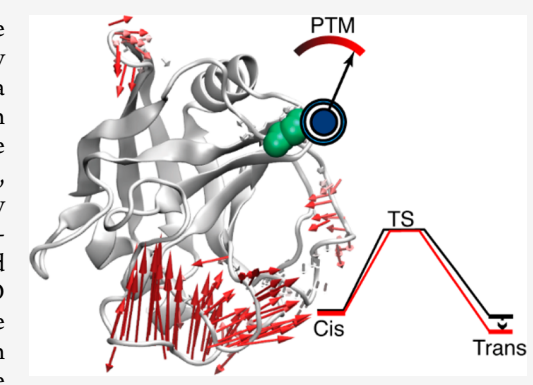
ACCESS

III Metrics & More

Article Recommendations

Supporting Information

ABSTRACT: Mitochondria are the powerhouse of a cell, whose disruption due to mitochondrial pore opening can cause cell death, leading to necrosis and many other diseases. The peptidyl-prolyl cis—trans isomerase cyclophilin D (CypD) is a key player in the regulation of the mitochondrial pore. The activity of CypD can be modulated by the post-translational modification (PTM). However, the detailed mechanism of this functional modulation is not well understood. Here, we investigate the catalytic mechanism of unmodified and modified CypD by calculating the reaction free energy profiles and characterizing the function-related conformational dynamics using molecular dynamics simulations and associated analyses. Our results show that unmodified and modified CypD considerably lower the isomerization free energy barrier compared to a free peptide substrate, supporting the catalytic activity of CypD in the simulation systems. The unmodified CypD reduces the free energy difference between the cis and trans states of the peptide substrate, suggesting a stronger binding affinity



of CypD toward *cis*, consistent with experiments. In contrast, phosphorylated CypD further stabilizes *trans*, leading to a lower catalytic rate in the *trans*-to-*cis* direction. The differential catalytic activities of the unmodified and phosphorylated CypD are due to a significant shift of the conformational ensemble upon phosphorylation under different functional states. Interestingly, the local flexibility is both reduced and enhanced at distinct regions by phosphorylation, which is explained by a "seesaw" model of flexibility modulation. The allosteric pathway between the phosphorylation site and a distal site displaying substantial conformational changes upon phosphorylation is also identified, which is influenced by the presence of the substrate or the substrate conformation. Similar conclusions are obtained for the acetylation of CypD using the same peptide substrate and the influence of substrate sequence is also examined. Our work may serve as the basis for the understanding of other PTMs and PTM-initiated allosteric regulations in CypD.

1. INTRODUCTION

Cyclophilin D (CypD), encoded by the PPIF gene, is a peptidyl-prolyl cis-trans isomerase and localized in mitochondria. A major function of CypD is to regulate mitochondrial permeability transition pore (mPTP). During the regulation of mPTP, CypD interacts with multiple mPTP components, including F1Fo-ATP synthase, phosphate carrier, and adenine nucleotide translocator.² The CypD-mPTP interaction is of pharmaceutical significance, since mPTP is involved in ischemia/reperfusion injury, neurodegenerative disorders, and muscular dystrophies. However, the detailed mechanism of the CypD mediated regulation of mPTP is not well understood. For example, under certain cellular conditions, CypD can undergo post-translational modifications (PTM) by surrounding enzymes, such as acetylases and kinases.2 These enzymes add functional groups to specific amino acid residues of CypD, leading to alteration of CypD function. Because of potential PTMs and other types of perturbation, such as mutation,

CypD exhibits contrasting regulatory roles and can both activate and inhibit pore opening.² An unanswered question is how do PTMs, which usually occur at a distal site to the active site of CypD, affect the catalytic activity?

The normal activity of CypD is to regulate the mPTP³ that in turn helps to keep the mitochondrion healthy. Due to oxidative stress or reperfusion injury, CypD can be phosphorylated, which causes a change in the activity that could lead to pore opening and cell death. Serine 191 (S191; residue number is based on the sequence unless indicated otherwise) is the major phosphorylation site of CypD involved

Received: August 30, 2022 Revised: November 25, 2022 Published: December 19, 2022





in mPTP regulation (Figure 1), although other serine sites are also suggested to be potential phosphorylation sites.⁴ Addi-

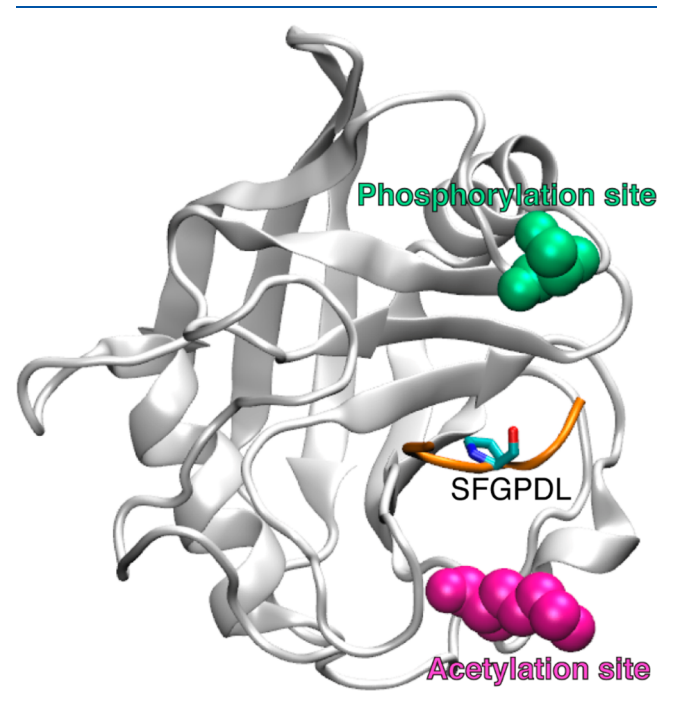


Figure 1. Crystal structure of CypD (Protein Data Bank (PDB) ID: 408H) with the peptide (SFGPDL). CypD is represented as a white cartoon, where the phosphorylation (S191 or S148 based on the PDB numbering) and acetylation (K167 or K124) sites are shown as spheres colored by green and purple, respectively. The phosphorylation and acetylation alter the enzyme activity leading to different physiological effects. The peptide (orange cartoon with the proline shown as sticks color coded by atom types) is modeled in the active site of CypD, and its *cis—trans* isomerization of the proline is simulated in both unmodified and modified CypD.

tionally, CypD can be acetylated at lysine 167 (K167) (Figure 1), and this modification also affects the activity of CypD.² For example, CypD acetylation causes the activation of mPTP that leads to cell death and age-related cardiac hypertrophy.⁵ Both S191 phosphorylation and K167 acetylation are reversible processes controlled by different enzymes during metabolism.⁶ Understanding the detailed mechanism of the function of modified and unmodified CypD has potential benefits in drug discovery. For example, it has been reported that cyclosporine (CsA) inhibits mPTP opening by binding to CypD.⁷ CsA is a strong binder not only to CypD but also to other cyclophilin isoforms. The intent of this study is to understand the mechanism of action of both unmodified and modified CypD that could contribute to the future development of new, isoform specific inhibitors.

Our main questions focus on understanding how PTMs, especially phosphorylation at S191, alter and regulate the catalytic activity of CypD. The phosphorylation of CypD has been studied recently. It has been shown that S191 phosphorylation, mediated by glycogen synthase kinase, increases the binding affinity of CypD to the Oligomycin Sensitivity-Conferring Protein (OSCP) subunit of ATP synthase, resulting in mPTP opening. CypD binding also reduces the enzymatic activity of ATP synthase, and phosphorylated CypD interacts with F1Fo-ATP synthase with a higher rate compared to unmodified CypD.

these studies, how PTMs allosterically affect the catalytic activity of CypD remains poorly understood. Described by want to characterize not only the consequence of the modification with respect to CypD catalysis but also the detailed mechanism of the allosteric process in terms of the modulation of conformational dynamics.

In this work, we report the free energy profiles of the isomerization process of the substrate and the allosteric mechanism of the unmodified and modified CypD. The catalytic activity of CypD can be assessed by measuring the relative free energy between states along the reaction coordinate (isomerization), including the transition state and the cis and trans states. For an enzyme to be efficient, it must lower the energy barrier between the transition state and the cis or trans state. We first characterize the free energy profiles of isomerization along the peptidyl-prolyl (omega) bond of the free peptide substrate and the substrate in the active sites of the unmodified CypD, S191 phosphorylated CypD, and K167 acetylated CypD (Figure 1). Our results suggest that phosphorylation of CypD stabilizes the trans conformation of the peptide substrate and hence generates a bias of catalysis for the cis-to-trans isomerization direction. We also combined normal molecular dynamics (MD) with advanced post simulation analysis methods to elucidate the allosteric mechanism due to the modification. Our study may serve as a basis to understand other PTMs of CypD, such as oxidation, palmitoylation, nitrosylation, and glutathionylation, which are known to play key roles in the mitochondrial regulation.² For example, CypD oxidation leads to mPTP induction, CypD nitrosylation leads to mPTP inhibition, CypD glutathionylation leads to stimulation of mitochondrial oxygen species and hypertension, and CypD S-palmitoylation leads to mPTP inhibition and reduces infarction.² Elucidating the effects of these PTMs would largely advance our understanding of critical subcellular processes.

2. COMPUTATIONAL METHODS

2.1. Preparation of Initial Structures. Initial coordinates of CypD were extracted from the PDB structure (PDB ID: 4O8H). 12 The models of the CypD-peptide complexes were generated based on previous studies. The protonation states of ionizable residues in CypD were determined as previously described¹⁴ and were kept the same for all simulation systems. The sequence of the peptide in the previous models was manually edited to match the current study (SFGPDL and SFAPDL), along with removing irrelevant side-chain atoms. The peptide SFGPDL (or its longer version analog) was used in previous computational and experimental studies showing that the isomerization of the peptide can be catalyzed by cyclophilins. The peptide sequence was derived based on the consensus of multiple cyclophilin targets and hence is a representative of cyclophilin substrates. 15-17 To test the sequence dependency, we mutated the P1 position of the peptide to alanine (i.e., SFAPDL). It has been shown that P1 primarily determines the substrate specificity of cyclophilins and prefers to be an alanine in the active site.¹⁸ Missing atoms were then added by the tLEaP program of AMBER 20.19 The peptide was capped by acetyl (ACE) and N-methylamide (NME) protecting groups to stabilize the system. Each system of free peptides and complexes for unmodified CypD (CypD), phosphorylated CypD (pCypD), and acetylated CypD (aCypD) was prepared in a similar manner. The phosphorylation was performed at

S191 of the CypD sequence (equivalent to S148 in the simulation system). The residue name SER was replaced by SEP to indicate the phosphorylated serine. The force field ff14SB²⁰ and the compatible force field for phosphorylated amino acids in AMBER 20¹⁹ were used to generate the phosphorylated protein-peptide topology files. The acetylation was performed at K167 of the CypD sequence (equivalent to K124 in the simulation system). The residue name LYS was changed into ALY to indicate the acetylated lysine. For acetylated systems, besides ff14SB,²⁰ the force field for the modified amino acids in AMBER 20¹⁹ was employed. The prepared initial models were used for both umbrella sampling (US) and normal MD simulations (see below). See Supplemental Table S1 for the list of all MD simulations and US calculations.

2.2. Umbrella Sampling. We performed umbrella sampling (US) based on molecular dynamics that provides the free energy along the reaction coordinate. The reaction coordinate is defined by the backbone ω torsional angle for the peptide Xaa-Pro, where Xaa is any amino acid preceding a proline and ω is defined by four atoms including C α and O of Xaa and $C\delta$ and $C\alpha$ of the proline. We calculated the free energy profile with ω being from -60° to 240° , a range that covers cis (0°) , transition state (90°) , and trans (180°) . The definition of the transition state being 90° has been established by our previous studies.^{21–25} US was applied as developed by Torrie and Valleau.²⁶ During the US, a bias potential was applied to the simulation system to maintain the ω angle around a specific value along the reaction coordinate. The systems were equilibrated before undergoing US in the same manner as in the normal MD (see section 2.3). Totally 61 windows were prepared for the reference ω range from -60° to 240° with an increment of 5°. For each window, an additional equilibration process was performed to prepare the system for the following production run of US. Specifically, starting from cis, series of MD simulations were performed, each for a total period of 1 ns under a harmonic dihedral restraint with the force constant of 0.01 kcal/(mol·deg²) and the reference angle being 0° , $\pm 5^{\circ}$, $\pm 10^{\circ}$, and so on. The conformation obtained at the end of the simulation for the current window was used as the starting point for the equilibration of the next window. Production simulations were performed in parallel under the same conditions as in the preparation step, except for the simulation time being 500 ns for each window (cumulatively 30.5 μ s for each system).

Following the US production simulations, the potential of mean force (PMF) was obtained using the weighted histogram analysis method (WHAM).²⁷ Specifically, the reaction coordinate was divided into 100 bins between the minimum (-60°) and the maximum (240°) . The value of 10^{-6} was used for the WHAM convergence tolerance. The WHAM calculations were performed at a temperature of 300 K. As a result, the free energy profile representing a function of ω was obtained for each system. The errors were estimated by Monte Carlo bootstrap, with the number of trials being 10 and the random seed 1234. The decorrelation time was set to be 1.2 ns. The parameter was determined based on an estimation of the correlation time being ~600 ps (Supplemental Figure S1), followed by the application of the empirical rule of using two folds of the correlation time to decorrelate data. Calculations were performed by using the WHAM program.²⁸

For each US calculation, we checked the stability of peptide binding during the production simulation for each window and

the overall PMF convergence. The complex was checked after each 60 ns to ensure that the proline of the peptide stayed inside the active site and was in the right orientation; otherwise, the last 60 ns was regenerated using the same initial conformation but different initial velocities. In checking the binding, the distance between the $C\alpha$ atoms of Arg 55 and the proline of the peptide was manually examined in the last snapshot of the 60 ns data visualized in VMD.²⁹ For the complex of the unmodified CypD and SFGPDL, the peptide proline showed no significant displacement out of the active site during the entire 500 ns simulation of all windows, indicating a tight binding. However, for other complexes including either modified CypD or SFAPDL (or both), significant proline displacement was observed in certain windows at certain time points (especially for the acetylated CypD, where the proline displacement occurred much earlier than other enzymes); for these cases, simulations were reperformed until the proline was stable in the active site. We also found that SFGPDL converged much faster than SFAPDL, consistent with the stability analysis showing that the glycine replacement enhanced the binding stability of the peptide toward the CypD active site. The convergence of PMF was inspected by checking the cumulative free energy difference between transition, cis, and trans states over time. We checked the convergence by using both forward and reverse cumulative averaging methods (Supplemental Figures S2 and S3).³⁰ We did not observe significant result changes after convergence in the reverse cumulative averaging (Supplemental Figure S3), suggesting that equilibration has little effect on the result.

2.3. Molecular Dynamics Simulations. The AMBER 20 suite of programs¹⁹ and the AMBER ff14SB force field parameters, ²⁰ a modified version of Cornell et al., ³¹ were used for the MD simulations. We reoptimized the ω -torsion angle parameters as previously demonstrated. 14,21 A periodic octahedron box filled with pre-equilibrated TIP3P water molecules was used to solvate the systems.³² A distance of at least 10 Å was set to separate the box faces from the solute. Water molecules from the crystallographic structure were kept as original. Na⁺ or Cl⁻ ions were used to neutralize the overall net charge of the systems. A total of 5,000 steps (3,000 steps of steepest descent and 2,000 steps of conjugate gradient) were applied to the systems for energy minimization. Harmonic restraints were applied to hold the positions of the solute atoms during energy minimization. The force constant of the positional restraint was gradually reduced from 500 to 0 kcal· mol⁻¹·Å⁻² during all five rounds of energy minimization. The systems were then heated up from 100 to 300 K (Langevin thermostat with collision frequency $\gamma = 1.0 \text{ ps}^{-1}$) within 500 ps under NVT conditions with a 1 fs time step and positional restraints to the solute. The force constant of restraint was set to 500, 300, 100, 50, and 5 kcal·mol⁻¹·Å⁻², respectively, during 5 rounds of heating. A 1 ns equilibration was performed for each system with a 2 fs time step and no restraint under NPT (300 K, 1 bar; Monte Carlo barostat with coupling constant τ_p = 1.0 ps). Each production simulation was performed for 2.2 μ s. Long-range electrostatic interactions were evaluated by the particle-mesh Ewald (PME) summation method.³³ Short-range nonbonded interactions were treated with a cutoff of 9 Å. SHAKE³⁴ algorithm was used to constrain all bonds involving hydrogen atoms and the simulation snapshots were saved every 1 ps.

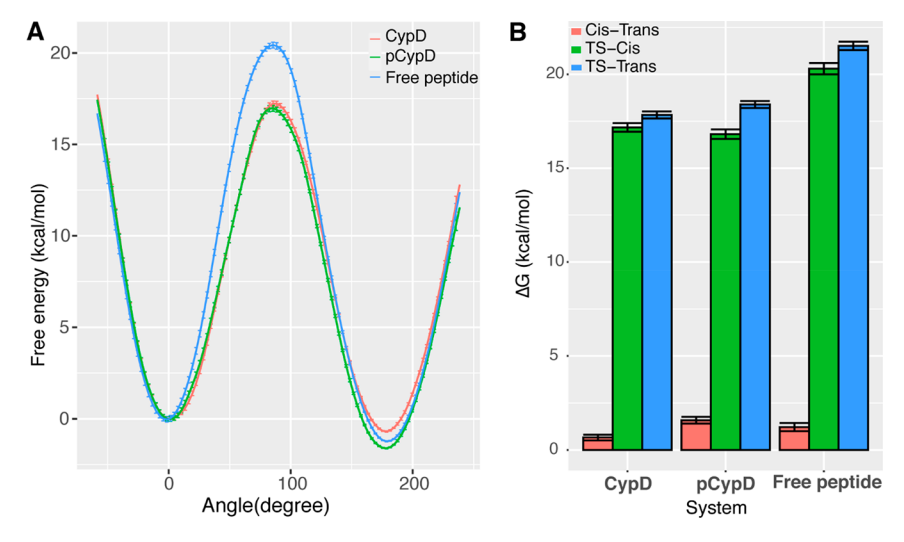


Figure 2. Potential of mean force (PMF) from US calculations. (A) PMF (or free energy) along the reaction coordinate. Three systems are presented: free peptide (i.e., SFGPDL), unmodified CypD-peptide complex (CypD), and phosphorylated CypD-peptide complex (pCypD). Error bars are estimated according to section 2.2. All lines are aligned by setting the free energy of cis (0°) to be 0 for easy comparisons. (B) Comparison of free energy changes from cis to the transition state or TS (TS-cis), from trans to TS (TS-trans), and from trans to cis (cis-trans) among the three systems. Detailed energy values are reported in Supplemental Table S2.

2.4. Principal Component Analysis (PCA) and Root-Mean-Square Fluctuation (RMSF). The CPPTRAJ program of AMBER 20 was used to perform PCA on trajectories derived from MD simulations.35 All the conformational snapshots were superimposed based on backbone atoms prior to the following steps. The calculation of eigenvalues and eigenvectors was performed based on the variancecovariance matrix representing the protein internal motions. A principal component (PC) is derived from the eigenvector, and the conformational variance is obtained from the eigenvalue. The first two PCs captured the most variance of the simulation trajectories, which were used to construct a 2D space to project all the simulated conformations for comparison. The "porcupine" plots were generated to represent the directions of the collective motions associated with the top PCs. The PC1-PC2 conformer plots were generated by ggplot2³⁶ and the porcupine plots were generated by VMD.²⁹ The RMSF was also performed to measure the flexibility of residues. CPPTRAJ was used to calculate RMSF and the Bio3D R package^{37–39} was used to analyze the results. The percentage change of RMSF was calculated as (RMSF_p -RMSF₁₁)/RMSF₁₁, where RMSF₂ is RMSF for phosphorylated CypD and RMSF_u is RMSF for the unmodified CypD. Changes of actual RMSF values were also calculated (Supplemental Figure S4), which show similar trends as the percentage changes.

2.5. Network Path Analysis. The difference contact network analysis (dCNA) based path analysis was performed to elucidate potential allosteric communication pathways as previously described. ⁴⁰ In brief, a protein structural network was constructed based on the residue-wise differential contact probabilities from the ensemble representing the unmodified to the ensemble representing the phosphorylated system. Networks were built for each pair of the systems under the apo, *cis*-substrate-bound, and *trans*-substrate-bound conditions. (Sub)optimal paths were searched between the phosphorylated residue (S191 or S148) and a distal residue that shows a large number of contact changes (residue D127 based on the numbering of the simulation system). For each network, 5,000

(sub)optimal paths were searched. All network edges were weighted by the change of contact strengths between the two distinct conformational ensembles. Network analyses were performed with Bio3D^{37–39} and in-house scripts. Molecular graphics were rendered by VMD.²⁹ All other figures were generated by ggplot2³⁶ and assembled by Illustrator (Adobe, Inc.).

3. RESULTS AND DISCUSSION

3.1. Post-Translational Phosphorylation of CypD Alters Recognition and Catalysis. We performed US of three systems, i.e., free peptide substrate, unmodified CypD/ peptide substrate complex, and phosphorylated CypD/peptide substrate complex (Figure 2). The trans conformation of all three systems has the lowest free energy. The free peptide substrate, SFGPDL, has the highest free energy barrier separating the trans and cis conformations of the -GPmotif, around 20.30 and 21.52 kcal/mol for cis-trans and trans-cis barriers, respectively, consistent with previous experimental and computational studies. 22,41,42 The unmodified enzyme reduces the energy barrier to around 17.17 and 17.83 kcal/mol for cis-trans and trans-cis, respectively. The modified enzyme (phosphorylated CypD or pCypD) stabilizes the trans state more than the unmodified enzyme, leading to energy barriers of around 16.81 and 18.39 kcal/mol for cistrans and trans-cis, respectively. Moreover, the free energy difference between cis and trans in the unmodified CypD is smaller than that in the free peptide, i.e., increase of the cis content in the enzyme-substrate complex (Figure 2B), suggesting a stronger binding affinity of CypD toward the cis peptide. In contrast, in pCypD, the energy difference is much larger than that in CypD, suggesting that the modified enzyme tends to bind the trans peptide better than unmodified CypD, reducing the *cis* content and increasing the free energy barrier from trans to cis.

The lowered free energy of the transition state in both unmodified and phosphorylated CypD indicates that both enzymes catalyze *cis—trans* isomerization, however, the pattern of the rate enhancement is different. For the direction from *cis*

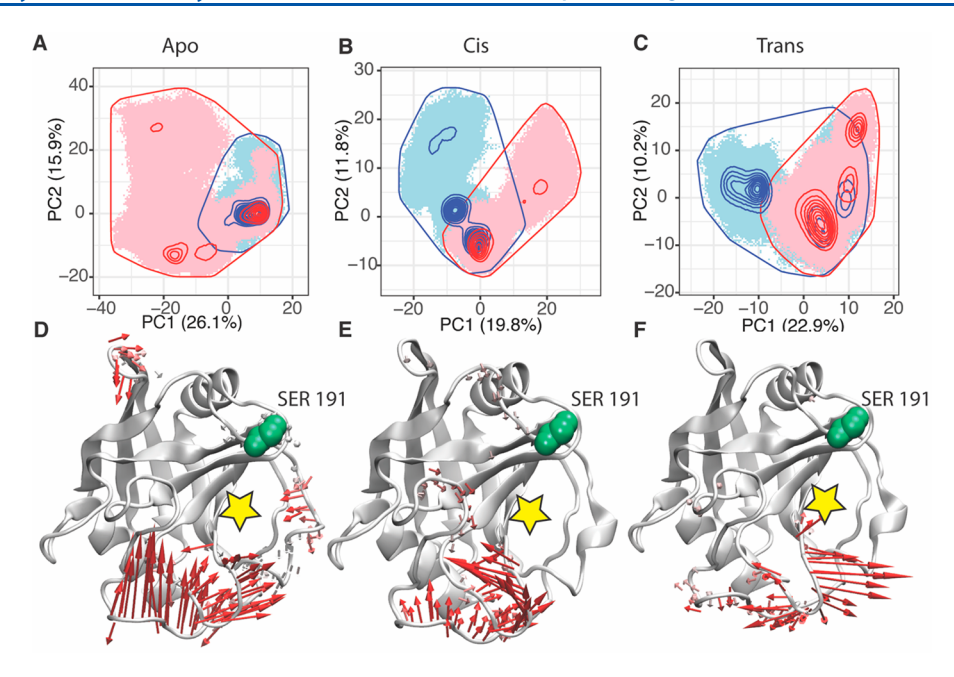


Figure 3. Principal component analysis reveals the shift of conformational ensemble upon phosphorylation under different substrate binding conditions. (A–C) PCA for the unmodified CypD (conformations in light blue and contour lines in blue) and phosphorylated CypD (pCypD; conformations in pink and contour lines in red). Contour lines represent probability density functions of conformations and the boundary of sampled space. (A) Apo condition, i.e., CypD without the peptide. (B) CypD bound with the peptide in the *cis* conformation. (C) CypD bound with the peptide in the *trans* conformation. Conformations are projected in the PC1–PC2 subspace that captures the highest percentage of variance. (D–F) Porcupine plot that shows the direction of PC1 motions for the three systems. Each arrow corresponds to the direction of motion of the atom along PC1. The magnitude of the arrow is determined by the loadings of the eigenvector for the corresponding atom and is scaled by the eigenvalue, i.e., the total variance captured by PC1. The yellow star indicates the active site.

to trans, the free energy barrier in pCypD is slightly lower $(\Delta \Delta G = 0.4 \text{ kcal/mol})$ than that in the unmodified CypD, indicating a slightly faster catalytic rate along this direction in pCypD, compared to the unmodified CypD. In contrast, for the direction from trans to cis, the unmodified CypD has a lower energy barrier ($\Delta \Delta G = 0.6 \text{ kcal/mol}$) and hence a faster catalytic rate along this direction, compared to pCypD (Figure 2B and Supplemental Table S2). We note that this work intends to understand the fine-tuning of protein function by PTMs, hence no dramatic energy difference is expected. The ~0.5 kcal/mol difference indicates a ~2-fold rate change of the isomerization, but cautions may be needed as different sources of errors, including the accuracy of the force field, may complicate the interpretation. The distinct catalytic activity between the unmodified and phosphorylated CypD might be attributed to their different roles in regulating mPTP opening. The phosphoresistant CypD mutant S191A has been shown to inhibit mPTP opening (and hence protects the mitochondrion), whereas the phosphomimetic CypD S191E mutant reversed such a (protective) effect and caused constant mPTP opening. We speculate that phosphorylation of CypD, causing a shift in the cis-trans relative stability of the substrate, may underlie the regulatory role of CypD in the sensitization of mPTP opening. We note that all the computational results here are rigorously checked with respect to convergence and accuracy (i.e., the stability of the protein-peptide complexes during simulations) (see section 2.2 and Supplemental Figures S2 and S3).

3.2. Modulation of the Conformational Ensemble of CypD Depends on Post-Translational Phosphorylation and the Isomeric States of the Substrate. Molecular dynamics simulations followed by trajectory analysis with PCA,

RMSF and network path analysis were performed to elucidate the detailed mechanism of how phosphorylation at S191 modifies the activity of CypD. Detailed changes of the conformational ensemble due to phosphorylation, under distinct substrate binding conditions, were examined. The dominant conformational substates of substrate-free CypD and pCypD (indicated by the dense conformational populations in Figure 3A) largely overlap. Phosphorylated CypD or pCypD samples a much larger conformational space with multiple less populated metastable substates, suggesting that phosphorylation enhances the overall flexibility (hence intrinsic conformational entropy) of the substrate-free enzyme while keeping the dominant conformational state unchanged. In contrast, phosphorylation of CypD causes an apparent shift of the conformational ensemble (in terms of the dominant or mean conformation) of the substrate-bound enzyme when the peptide in the cis (Figure 3B) or the trans (Figure 3C) state is bound to pCypD. Phosphorylated CypD or pCypD samples a smaller conformational space in the complexes, compared to the substrate-free pCypD, suggesting a reduction of CypD flexibility upon substrate binding. This loss of entropy is partly compensated for by the increase in flexibility (entropy) of the peptide (see section 3.3). We observe that the trans peptide bound pCypD has more conformational substates than that bound with the *cis* peptide, which indicates that the protein is more flexible when it is bound to the trans configuration of the substrate. This might explain the higher binding affinity of pCypD for the trans configuration of the substrate (see section 3.1). Our results suggest that phosphorylation modifies the conformational ensemble of CypD, and details of the modification depend on whether the peptide substrate is bound to the enzyme and the prolyl isomeric state of the

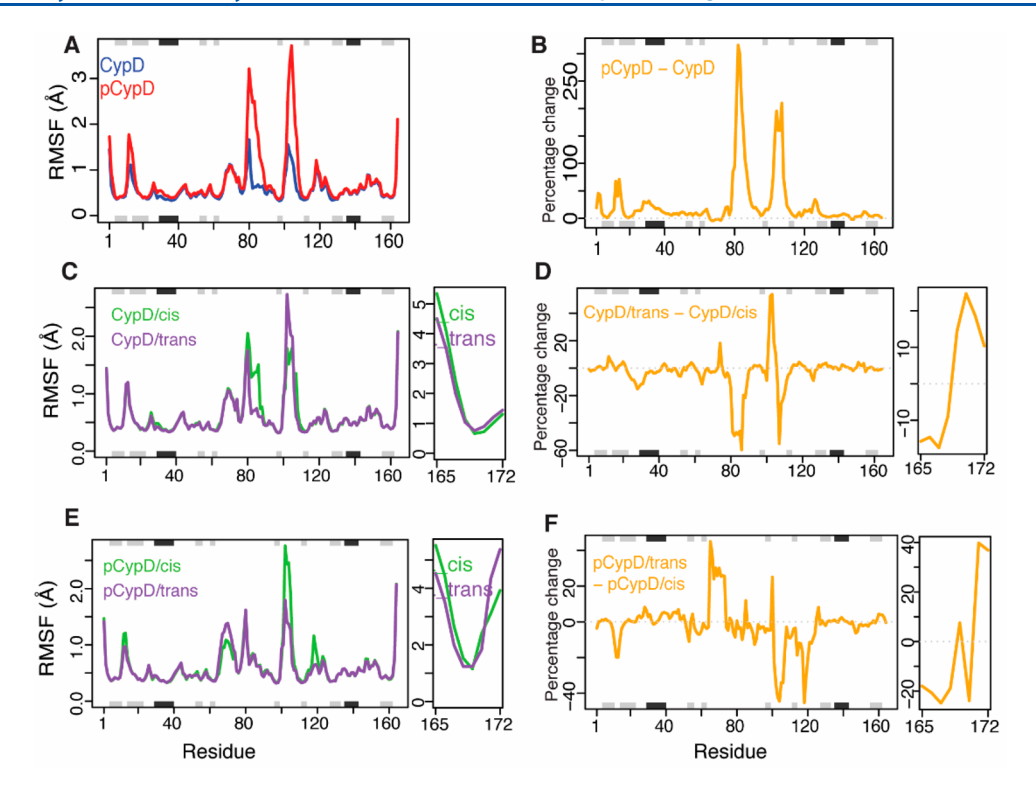


Figure 4. Root mean square fluctuation that shows the flexibility of residues before and after the phosphorylation under different substrate binding conditions. (A, B) RMSF and differential RMSF comparing the unmodified and the phosphorylated CypD in the absence of the substrate peptide. The differential RMSF shows how the RMSF changes from unmodified CypD to pCypD, in the unit of percentage change (see section 2.4). (C, D) RMSF and differential RMSF of unmodified CypD in complex with the substrate. The differential RMSF is calculated following the isomerization direction from *cis* to *trans* conformational states. (E, F) RMSF and differential RMSF of the phosphorylated CypD in complex with the substrate in different isomeric states. In C–F, the plot for the peptide is separated from that of the enzyme. The black and gray rectangles on the top and bottom of each plot represent α-helices and β-strands, respectively.

bound substrate. PTM of the enzyme triggers regional conformational changes distal to the phosphorylation site by shifting the conformational ensemble, which may form the dynamic basis for the allosteric effect in CypD.

Although modulation of the conformational ensemble due to phosphorylation is different between the substrate-free and substrate-bound states of the enzyme, the structural regions modulated are largely consistent. Interestingly, in all the three systems, phosphorylation mainly alters the dynamics at a distal site around residues 70-120 (numbering based on the simulation system; Figure 3D-F), indicating an allosteric effect of the PTM. These loops are around the "gatekeeper" region of substrate binding, 43 and modulation of the dynamics in the region may affect binding affinity and catalysis. In the cissubstrate-bound complexes, the dominant collective motions (large red arrows in Figure 3E) show a closing of the binding site around the gatekeeper from the unmodified CypD to pCypD, suggesting a relatively unfavorable binding of the substrate in the cis configuration to pCypD. In contrast, in the trans-substrate-bound complexes, the motions are opposite, suggesting that the substrate in the trans configuration binds pCypD better than CypD. These are consistent with our free energy calculations, where pCypD shows a significantly larger bias toward binding the substrate in the trans configuration (see section 3.1).

3.3. A "Seesaw" Model for the Modification of Flexibility in Major Loops Across CypD Generated by Phosphorylation. The root-mean-square fluctuation (RMSF) results of the backbone of CypD and pCypD provide

more detailed understanding of the effect of phosphorylation (Figure 4 and Supplemental Figure S4). Under the substrate-free condition, pCypD is much more flexible than the unmodified CypD, and major changes are observed in loops comprising residues 70–90 (numbering based on the simulation system) and 100–120 (Figure 4A,B and Supplemental Figure S4). Substrate binding suppresses the fluctuations in these major loops in pCypD, leading to a similar overall flexibility between pCypD and unmodified CypD (Figure 4C–F and Supplemental Figure S4). The reduced pCypD flexibility by substrate binding is partly compensated for by the large fluctuation at the N- and C-terminal halves of the substrate (Figure 4C,E).

Changes in the RMSF from trans- to cis-substrate-bound phosphorylated complexes suggest a "seesaw model" (Figure 4E,F and Supplemental Figure S4), where the increase or decrease of fluctuation at one region is compensated for by the opposite change of fluctuation at another region. For example, the trans-substrate-bound pCypD has a lower RMSF than the cis bound pCypD at around residues 100-120 (numbering based on the simulation system), and this difference is compensated for by the reverse change at around residues 60-80 (Figure 4E,F and Supplemental Figure S4). In contrast, in the unmodified CypD (Figure 4C,D and Supplemental Figure S4), the dynamic modulation is primarily stabilization of RMSF from cis to trans at around residue 80. CypD has both increase and decrease of RMSF at around residues 100-120, but mainly RMSF increase (from cis to trans) at around 100 (Figure 4D and Supplemental Figure S4). The loop around

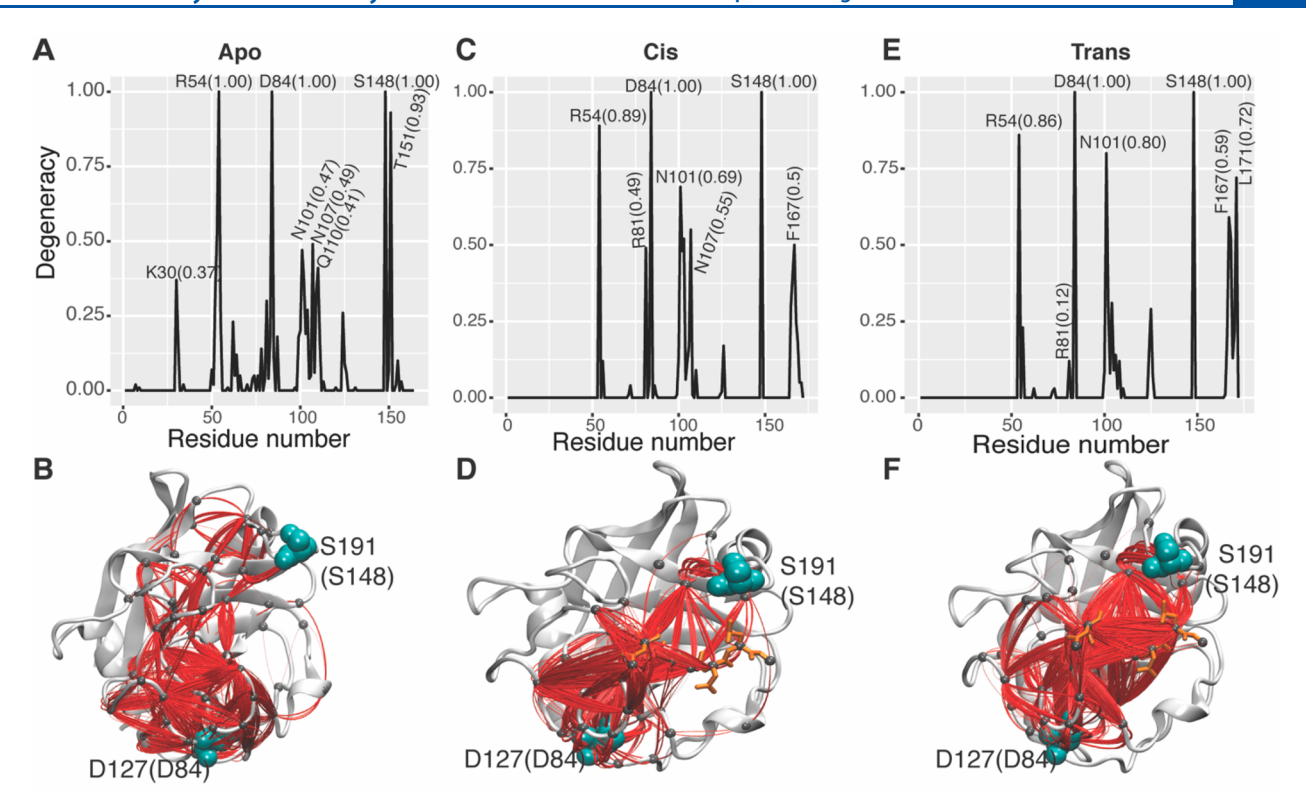


Figure 5. Path analysis shows how the allosteric signal is transmitted through the protein due to the phosphorylation. (A, C, and E) Normalized node degeneracy over 5000 (sub)optimal paths for each system. (B, D, and F) Paths that are represented in colored lines with radii of the paths scaled by path lengths. CypD is represented as white cartoon. The "source" and "sink" residues used in the path analysis are represented as cyan spheres. The substrate peptide (D, F) is shown as orange sticks. Dark gray small spheres indicate residues that have a nonzero node degeneracy.

residue 100 constitutes part of the substrate binding site and is known to be critical for the catalytic function. ¹³ The opposite dynamic modulations around this loop in CypD and pCypD correlate with the opposite binding preferences of substrate conformation in these two enzymes (i.e., CypD binds the *cis* substrate better whereas pCypD binds *trans* better).

3.4. Phosphorylation Triggers Allosteric Communi**cations via Specific Residues.** We identified critical residues that define the allosteric pathways from one protein region to another using the (sub)optimal path analysis within the dCNA framework (Figure 5).40 In dCNA, a protein structural network is built where the nodes are amino acid residues and edges represent residue-residue contact changes following phosphorylation. The path analysis is then performed to identify key residues that play a role in the allosteric communication between residues S191 (the phosphorylation site; equivalent to S148 of the simulation system) and D127 (a distal site showing substantial residue-residue contact changes; equivalent to D84 of the simulation system). The normalized node degeneracy (i.e., the fraction of the number of paths going through each residue) is used to measure the importance of the residue for the allosteric communication (see Figure 5A for an example; see Supplemental Table S3 for the table of all degeneracies). The two end nodes S191 (or S148) and D127 (D84) (i.e., the so-called "source and sink") always have degeneracies of 1 as all paths go through them. Figure 5 shows that, beginning from the phosphorylation site, the allosteric signal visits different residues until it reaches the distal site, and the traveling paths are localized on one side of the enzyme. The paths between the two substrate-bound forms of the enzyme are more similar compared to those between the

substrate-free and substrate-bound forms. The major difference is that in the substrate-bound forms, the substrate peptide is also utilized as a bridge for the allosteric communication (Figure 5C,E, respectively, for the *cis* and *trans* peptide); between the substrate-bound forms, however, small deviations of paths are also observed (Figure 5D,F).

Despite the divergent allosteric pathways, some common residues responsible for mediating the allosteric effects from the unmodified to the phosphorylated CypD are identified for the apo, cis-bound, and trans-bound systems. For example, the key active-site residue R54 and the gatekeeper residues R81, N101, and A102 all have a significant degeneracy (>0.1) for all the systems (Supplemental Table S3). These residues are expected to be critical for the allosteric transition, initiated by S191 phosphorylation, in CypD regardless of the substrate binding condition. The concurrence of importance for both function and allosteric regulation in these residues indicates that phosphorylation allosterically affects the enzyme activity. It is also interesting to point out that although all the systems have the loop around the residue N101 be part of the allosteric pathway, the pathway is concentrated in fewer residues in the complexes than that in the apo system (Figure 5A,C,E and Supplemental Table S3). Moreover, the average path lengths of apo, cis-bound, and trans-bound systems being 17.2, 9.5, and 12.1, respectively, suggest slightly different efficiencies in the allosteric communication among the three systems. These results provide an example of the fine-tuning of the allosteric pathway by substrate binding.

3.5. Effects of CypD Acetylation and Peptide Sequence Dependency. Besides phosphorylation, we examined the effect of acetylation of CypD on the enzyme

catalysis. The acetylation modification occurs at K167, i.e., K124 based on the numbering of the simulation system. Our free energy profile results indicate that, like phosphorylation, CypD acetylation leads to a more stable *trans* conformation compared to the free peptide (Supplemental Figure S5). It has been shown that acetylation of CypD in the hippocampus triggered the opening of mPTP, and CypD deacetylation by SIRT3 inhibited mPTP opening. He is yet to unveil the detailed mechanism of how the transition between *trans* and *cis* conformations regulates pore opening, although an interesting hypothesis has been proposed. He

We also tested how the substrate peptide sequence may influence the results (Supplemental Figure S6). We replaced the glycine preceding the proline in the peptide (SFGPDL) with an alanine (SFAPDL). It shows that substrate binding to the enzyme is sequence dependent. Glycine is more flexible than alanine, and the replacement causes the substrate to stay in the active site less tightly, which may lead to a less efficient catalysis. While SFGPDL is the most stable in the trans conformation in the unmodified CypD, the alanine substitution causes a shift of stability toward cis (see Supplemental Figure S6B) and preferred direction of catalysis toward transto-cis. Hence, we speculate that the unmodified CypD tends to stabilize the cis conformation of the substrate, although the magnitude of the stabilization, which can lead to an alteration of the preferred catalytic direction, depends on the sequence of the substrate. However, the effect of modification remains the same between the peptides. Both pCypD and aCypD show a much more stabilized trans conformation (Supplemental Figure S6C,D) of the SFAPDL peptide than the unmodified CypD, a phenomenon also observed in using the SFGPDL peptide. Also, in contrast to the unmodified CypD, both modified enzymes prefer the cis-to-trans direction of catalysis regardless of the sequence of the substrate.

4. CONCLUSIONS

In this study, we performed umbrella sampling, molecular dynamics, and associated analyses to study the effect of posttranslational modification on CypD catalysis. Umbrella sampling enables the sampling of low-probability regions along the reaction coordinate and provides a way to characterize the free energy profile of the system during the cis-trans isomerization of the peptide substrate. The results of the free energy profiles suggest that phosphorylation and acetylation of CypD could stabilize the trans conformation of mPTP proteins in mitochondria, possibly responsible for opening the mPTP. Normal MD along with PCA and RMSF analyses showed global and local conformational changes, respectively, due to the phosphorylation under different substrate binding conditions, suggesting allosteric effects by the modification. A seesaw model is proposed to explain the dynamic modulation, where the change of flexibility in one region is compensated for by the opposite change of flexibility in a distinct region. We also applied our newly developed method, dCNA based (sub)optimal path analysis, to quantify the allosteric effects generated across CypD due to the phosphorylation. The path analysis identifies residues that are crucial for the allosteric communication. The path analysis reveals different intrinsic allosteric pathways for different substrate binding conditions, including the involvement of peptide in bridging the pathway in the complexes. Common allosteric residues among the systems are also identified, which are found to be near functional sites. Our work may serve as

the basis for the understanding of other PTMs in CypD, such as those occurring at cysteine 202 including nitrosylation, palmitoylation, oxidation, and acylation. A critical issue here is to identify appropriate force fields for these modified systems. Such extensive understanding of PTMs will allow us to gain unprecedented insights into the function of CypD and may facilitate the design of new potential therapeutics targeting CypD or related pathways in the future.

ASSOCIATED CONTENT

Supporting Information

The Supporting Information is available free of charge at https://pubs.acs.org/doi/10.1021/acs.jpcb.2c06208.

Example autocorrelation function over the lag of time; convergence of free energy calculations using the forward cumulative averaging method and the reverse cumulative averaging method; differential RMSF between different systems; potential of mean force (PMF) for the acetylated CypD using the SFGPDL peptide and for the free SFAPDL peptide and the peptide in complex with unmodified and modified CypD; list of US and MD simulations; average free energies (kcal/mol) at 500 ns for *cis*, transition state (TS), and *trans* for each system using the SFGPDL peptide; degeneracies of the path analysis (PDF)

AUTHOR INFORMATION

Corresponding Author

Donald Hamelberg — Department of Chemistry and Center for Diagnostics and Therapeutics, Georgia State University, Atlanta, Georgia 30302-3965, United States; ⊚ orcid.org/0000-0002-3785-3037; Phone: (404) 413-5564; Email: dhamelberg@gsu.edu

Authors

Jacques Kumutima — Department of Chemistry and Center for Diagnostics and Therapeutics, Georgia State University, Atlanta, Georgia 30302-3965, United States Xin-Qiu Yao — Department of Chemistry, Georgia State University, Atlanta, Georgia 30302-3965, United States;

Complete contact information is available at: https://pubs.acs.org/10.1021/acs.jpcb.2c06208

orcid.org/0000-0003-2706-2028

Notes

The authors declare no competing financial interest.

ACKNOWLEDGMENTS

This research was supported by the National Science Foundation (MCB-2018144) and the Georgia Research Alliance. J.K. acknowledges the fellowship from the Center for Diagnostics and Therapeutics (CDT) of Georgia State University. This work used the Advanced Research Computing Technology and Innovation Core (ARCTIC) resources, which is supported by the National Science Foundation Major Research Instrumentation (MRI) grant no. CNS-1920024. We acknowledge the use of Georgia State's research computing resources that are supported by Georgia State's Research Solutions.

REFERENCES

- (1) Lin, D. T.; Lechleiter, J. D. Mitochondrial targeted cyclophilin D protects cells from cell death by peptidyl prolyl isomerization. *J. Biol. Chem.* **2002**, 277, 31134–31141.
- (2) Amanakis, G.; Murphy, E. Cyclophilin D: An Integrator of Mitochondrial Function. *Front. Physiol.* **2020**, *11*, 595.
- (3) Teodoro, J. S.; Varela, A. T.; Duarte, F. V.; Gomes, A. P.; Palmeira, C. M.; Rolo, A. P. Indirubin and NAD(+) prevent mitochondrial ischaemia/reperfusion damage in fatty livers. *Eur. J. Clin Invest* **2018**, 48, e12932.
- (4) Hurst, S.; Gonnot, F.; Dia, M.; Crola Da Silva, C.; Gomez, L.; Sheu, S.-S. Phosphorylation of cyclophilin D at serine 191 regulates mitochondrial permeability transition pore opening and cell death after ischemia-reperfusion. *Cell Death Dis.* **2020**, *11*, 661.
- (5) Hafner, A. V.; Dai, J.; Gomes, A. P.; Xiao, C. Y.; Palmeira, C. M.; Rosenzweig, A.; Sinclair, D. A. Regulation of the mPTP by SIRT3-mediated deacetylation of CypD at lysine 166 suppresses age-related cardiac hypertrophy. *Aging (Albany NY)* **2010**, *2*, 914–923.
- (6) Lu, Z.; Scott, I.; Webster, B. R.; Sack, M. N. The emerging characterization of lysine residue deacetylation on the modulation of mitochondrial function and cardiovascular biology. *Circ. Res.* **2009**, 105, 830–841.
- (7) Connern, C. P.; Halestrap, A. P. Purification and N-terminal sequencing of peptidyl-prolyl cis-trans-isomerase from rat liver mitochondrial matrix reveals the existence of a distinct mitochondrial cyclophilin. *Biochem. J.* **1992**, *284*, 381–385.
- (8) Dhingra, R.; Lieberman, B.; Kirshenbaum, L. A. Cyclophilin D phosphorylation is critical for mitochondrial calcium uniporter regulated permeability transition pore sensitivity. *Cardiovasc. Res.* **2019**, *115*, 261–263.
- (9) Rasola, A.; Sciacovelli, M.; Chiara, F.; Pantic, B.; Brusilow, W. S.; Bernardi, P. Activation of mitochondrial ERK protects cancer cells from death through inhibition of the permeability transition. *Proc. Natl. Acad. Sci. U. S. A.* **2010**, *107*, 726–731.
- (10) Giorgio, V.; Bisetto, E.; Soriano, M. E.; Dabbeni-Sala, F.; Basso, E.; Petronilli, V.; Forte, M. A.; Bernardi, P.; Lippe, G. Cyclophilin D modulates mitochondrial F0F1-ATP synthase by interacting with the lateral stalk of the complex. *J. Biol. Chem.* **2009**, *284*, 33982–33988.
- (11) Wapeesittipan, P.; Mey, A.; Walkinshaw, M.; Michel, J. Allosteric effects in cyclophilin mutants may be explained by changes in nano-microsecond time scale motions. *Commun. Chem.* **2019**, *2*, 41.
- (12) Valasani, K. R.; Carlson, E. A.; Battaile, K. P.; Bisson, A.; Wang, C.; Lovell, S.; Yan, S. S. High-resolution crystal structures of two crystal forms of human cyclophilin D in complex with PEG 400 molecules. *Acta Crystallogr., Sect. F: Struct. Biol. Cryst. Commun.* 2014, 70, 717–722
- (13) Vu, P. J.; Yao, X.-Q.; Momin, M.; Hamelberg, D. Unraveling Allosteric Mechanisms of Enzymatic Catalysis with an Evolutionary Analysis of Residue—Residue Contact Dynamical Changes. *ACS Catal.* **2018**, *8*, 2375–2384.
- (14) Kumutima, J.; Yao, X. Q.; Hamelberg, D. p53 Is Potentially Regulated by Cyclophilin D in the Triple-Proline Loop of the DNA Binding Domain. *Biochemistry* **2021**, *60*, 597–606.
- (15) Doshi, U.; Holliday, M. J.; Eisenmesser, E. Z.; Hamelberg, D. Dynamical network of residue-residue contacts reveals coupled allosteric effects in recognition, catalysis, and mutation. *Proc. Natl. Acad. Sci. U. S. A.* **2016**, *113*, 4735–4740.
- (16) Piotukh, K.; Gu, W.; Kofler, M.; Labudde, D.; Helms, V.; Freund, C. Cyclophilin A binds to linear peptide motifs containing a consensus that is present in many human proteins. *J. Biol. Chem.* **2005**, 280, 23668–23674.
- (17) Holliday, M. J.; Camilloni, C.; Armstrong, G. S.; Isern, N. G.; Zhang, F.; Vendruscolo, M.; Eisenmesser, E. Z. Structure and Dynamics of GeoCyp: A Thermophilic Cyclophilin with a Novel Substrate Binding Mechanism That Functions Efficiently at Low Temperatures. *Biochemistry* **2015**, *54*, 3207–3217.
- (18) Zoldak, G.; Aumuller, T.; Lucke, C.; Hritz, J.; Oostenbrink, C.; Fischer, G.; Schmid, F. X. A library of fluorescent peptides for

- exploring the substrate specificities of prolyl isomerases. *Biochemistry* **2009**, *48*, 10423–10436.
- (19) Case, D. A.; Walker, R. C.; Cheatham, T. E., III; Simmerling, C.; Roitbert, A.; Merz, K. M.; Luo, R.; Li, P.; Darden, T.; Sagui, C. et al. *AMBER* 2021; University of California: San Francisco, 2021.
- (20) Maier, J. A.; Martinez, C.; Kasavajhala, K.; Wickstrom, L.; Hauser, K. E.; Simmerling, C. ff14SB: Improving the Accuracy of Protein Side Chain and Backbone Parameters from ff99SB. *J. Chem. Theory Comput.* **2015**, *11*, 3696–3713.
- (21) Doshi, U.; Hamelberg, D. Reoptimization of the AMBER Force Field Parameters for Peptide Bond (Omega) Torsions Using Accelerated Molecular Dynamics. *J. Phys. Chem. B* **2009**, *113*, 16590–16595.
- (22) Doshi, U.; McGowan, L. C.; Ladani, S. T.; Hamelberg, D. Resolving the complex role of enzyme conformational dynamics in catalytic function. *Proc. Natl. Acad. Sci. U.S.A.* **2012**, *109*, 5699–5704.
- (23) Ladani, S. T.; Hamelberg, D. Entropic and Surprisingly Small Intramolecular Polarization Effects in the Mechanism of Cyclophilin A. J. Phys. Chem. B **2012**, 116, 10771–10778.
- (24) Tork Ladani, S.; Hamelberg, D. Intricacies of interactions, dynamics and solvent effects in enzyme catalysis: a computational perspective on cyclophilin A. *Mol. Simul.* **2014**, *40*, 765–776.
- (25) Tork Ladani, S.; Souffrant, M. G.; Barman, A.; Hamelberg, D. Computational perspective and evaluation of plausible catalytic mechanisms of peptidyl-prolyl cis-trans isomerases. *Biochim. Biophys. Acta* **2015**, *1850*, 1994–2004.
- (26) Torrie, G. M.; Valleau, J. P. Nonphysical sampling distributions in Monte Carlo free-energy estimation: Umbrella sampling. *J. Comput. Phys.* **1977**, 23, 187–199.
- (27) Kumar, S.; Rosenberg, J. M.; Bouzida, D.; Swendsen, R. H.; Kollman, P. A. THE weighted histogram analysis method for free-energy calculations on biomolecules. I. The method. *J. Comput. Chem.* **1992**, *13*, 1011–1021.
- (28) Grossfield, A. WHAM: The Weighted Histogram Analysis Method, version 2.0. http://membrane.urmc.rochester.edu/wordpress/?page id=126.
- (29) Humphrey, W.; Dalke, A.; Schulten, K. VMD: Visual Molecular Dynamics. *J. Mol. Graph.* **1996**, *14*, 33–38.
- (30) Yang, W.; Bitetti-Putzer, R.; Karplus, M. Free energy simulations: use of reverse cumulative averaging to determine the equilibrated region and the time required for convergence. *J. Chem. Phys.* **2004**, 120, 2618–2628.
- (31) Cornell, W. D.; Cieplak, P.; Bayly, C. I.; Gould, I. R.; Merz, K. M.; Ferguson, D. M.; Spellmeyer, D. C.; Fox, T.; Caldwell, J. W.; Kollman, P. A. A Second Generation Force Field for the Simulation of Proteins, Nucleic Acids, and Organic Molecules. *J. Am. Chem. Soc.* 1996, 118, 2309–2309.
- (32) Mark, P.; Nilsson, L. Structure and Dynamics of the TIP3P, SPC, and SPC/E Water Models at 298 K. J. Phys. Chem. A 2001, 105, 9954–9960.
- (33) Darden, T.; York, D.; Pedersen, L. Particle mesh Ewald: An Nlog(N) method for Ewald sums in large systems. *J. Chem. Phys.* **1993**, 98, 10089–10092.
- (34) Ryckaert, J.-P.; Ciccotti, G.; Berendsen, H. J. C. Numerical integration of the cartesian equations of motion of a system with constraints: molecular dynamics of n-alkanes. *J. Comput. Phys.* **1977**, 23, 327–341.
- (35) Roe, D. R.; Cheatham, T. E. PTRAJ and CPPTRAJ: Software for Processing and Analysis of Molecular Dynamics Trajectory Data. *J. Chem. Theory Comput.* **2013**, *9*, 3084–3095.
- (36) Wickham, H. ggplot2: elegant graphics for data analysis; Springer, 2016.
- (37) Grant, B. J.; Rodrigues, A. P.; ElSawy, K. M.; McCammon, J. A.; Caves, L. S. Bio3d: an R package for the comparative analysis of protein structures. *Bioinformatics* **2006**, *22*, 2695–2696.
- (38) Skjærven, L.; Yao, X.-Q.; Scarabelli, G.; Grant, B. J. Integrating protein structural dynamics and evolutionary analysis with Bio3D. *BMC Bioinf.* **2014**, *15*, 399.

- (39) Grant, B. J.; Skjærven, L.; Yao, X.-Q. The Bio3D packages for structural bioinformatics. Protein Sci. 2021, 30, 20-30.
- (40) Yao, X. Q.; Hamelberg, D. Residue-Residue Contact Changes during Functional Processes Define Allosteric Communication Pathways. J. Chem. Theory Comput. 2022, 18, 1173-1187.
- (41) Grathwohl, C.; Wüthrich, K. Nmr studies of the rates of proline cis-trans isomerization in oligopeptides. Biopolymers 1981, 20, 2623-2633.
- (42) Beausoleil, E.; Lubell, W. D. Steric Effects on the Amide Isomer Equilibrium of Prolyl Peptides. Synthesis and Conformational Analysis of N-Acetyl-5-tert-butylproline N'-Methylamides. J. Am. Chem. Soc. 1996, 118, 12902-12908.
- (43) Davis, T. L.; Walker, J. R.; Campagna-Slater, V.; Finerty, P. J.; Paramanathan, R.; Bernstein, G.; MacKenzie, F.; Tempel, W.; Ouyang, H.; Lee, W. H.; et al. Structural and biochemical characterization of the human cyclophilin family of peptidyl-prolyl isomerases. PLoS Biol. 2010, 8, e1000439.
- (44) Sun, F.; Si, Y.; Bao, H.; Xu, Y.; Pan, X.; Zeng, L.; Jing, L. Regulation of Sirtuin 3-Mediated Deacetylation of Cyclophilin D Attenuated Cognitive Dysfunction Induced by Sepsis-Associated Encephalopathy in Mice. Cell Mol. Neurobiol 2017, 37, 1457-1464.
- (45) Nesci, S. Protein folding and unfolding: proline cis-trans isomerization at the c subunits of F1 FO -ATPase might open a high conductance ion channel. Proteins 2022, 90, 2001-2005.

□ Recommended by ACS

Rare Catechol-O-methyltransferase Missense Variants Are **Structurally Unstable Proteasome Targets**

Fia B. Larsen, Rasmus Hartmann-Petersen, et al.

MARCH 28 2023 **BIOCHEMISTRY**

READ **Z**

Molecular Insights into the Heterotropic Allosteric Mechanism in Cytochrome P450 3A4-Mediated Midazolam Metabolism

Tingting Fu, Qingchuan Zheng, et al.

NOVEMBER 07, 2022

JOURNAL OF CHEMICAL INFORMATION AND MODELING

READ M

Computation-Aided Engineering of Cytochrome P450 for the **Production of Pravastatin**

Mark A. Ashworth, Andrew W. Munro, et al.

NOVEMBER 28, 2022

ACS CATALYSIS

RFAD 17

Cooperative Substrate Binding Controls Catalysis in Bacterial Cytochrome P450terp (CYP108A1)

Jessica A. Gable, Alec H. Follmer, et al.

FEBRUARY 13, 2023

JOURNAL OF THE AMERICAN CHEMICAL SOCIETY

READ **C**

Get More Suggestions >